LANGMUIR

Article

pubs.acs.org/Langmuir

Understanding the Interaction of Pluronics L61 and L64 with a DOPC Lipid Bilayer: An Atomistic Molecular Dynamics Study

Nazar Ileri Ercan,[†,‡,§] Pieter Stroeve,[†] Joseph W. Tringe,[‡] and Roland Faller*[,†]

[†]Chemical Engineering Department, University of California, Davis, One Shields Avenue, Davis, California 95616, United States

[‡]Lawrence Livermore National Laboratory, 7000 East Avenue, Livermore, California 94551, United States

[§]Chemical Engineering Department, Bogazici University, Bebek, 34342 Istanbul, Turkey

ABSTRACT: We investigate the interactions of Pluronics L61 and L64 with a dioleylphosphatidylcholine (DOPC) lipid bilayer by atomistic molecular dynamics simulations using the all-atom OPLS force field. Our results show that the initial configuration of the polymer with respect to the bilayer determines its final conformation within the bilayer. When the polymer is initially placed at the lipid/water interface, we observe partial insertion of the polymer in a U-shaped conformation. On the other hand, when the polymer is centered at the bilayer, it stabilizes to a transmembrane state, which facilitates water transport across the bilayer. We show that membrane thickness decreases while its fluidity increases in the presence of Pluronics. When the polymer concentration inside the bilayer is high, pore formation is initiated with L64. Our results show good agreement with existing experimental data and reveal that the hydrophilic/lipophilic balance of the polymer plays a critical role in the interaction mechanisms as well as in the dynamics of Pluronics with and within the bilayer.

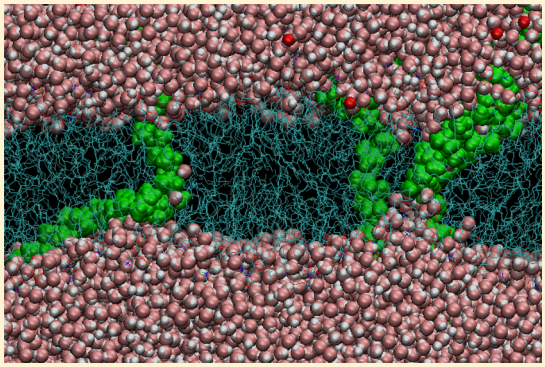

INTRODUCTION

Amphiphilic block copolymers have been of great interest for pharmaceutics and biomedicine, not only as drug nanocarrier components but also as elements with therapeutic activity.[1−3] These copolymers can target specific cells in the body[4] and control cellular and physiological responses.[5,6] A specific type of amphiphilic triblock copolymers is Pluronics, also known as poloxamers or symperonics, that consist of a hydrophobic poly(propylene oxide) (PPO) block connected to hydrophilic poly(ethylene oxide) (PEO) blocks at each end. Pluronics display exceptional biological activities; e.g., they have been shown to enhance gene transcription[7] and increase the sensitivity of multidrug resistant cells *in vitro* and *in vivo*.[8] They can seal damaged cell membranes and restore cell integrity[2,9] or facilitate the passage of molecules across lipid membranes and increase membrane permeability.[10−12] The PEO and PPO block size determines the hydrophilic−lipophilic balance (HLB) of the copolymer and hence its biological activity or, more specifically, its degree of association with the cell membrane.[13] Hydrophilic parts of the polymer prefer to interact with polar heads of the membrane, whereas the PPO blocks are repelled. These opposing interactions can result in polymer localization at the interface or partial/full insertion into the membrane and hence change the membrane properties. To design effective nanomedicines, it is important to understand these interactions and the underlying molecular mechanisms in detail. Several experimental studies have been conducted in this context using different types of Pluronics, membrane models (monolayers,[14] bilayers,[15,16] liposomes,[9,17] and cells[18]), and experimental methods including fluorescence microscopy,[14] X-ray scattering and differential scanning calorimetry,[15,17,19] dynamic nuclear polarization,[9] and micro-cantilever sensing.[16] Most of these studies indicate that the association of Pluronics with the lipid membranes depends on the length of the PPO block, hydrophilicity of the copolymer, membrane type, and membrane composition. In addition, temperature can play an important role on the solubility of the polymer in the membranes.[16] Experiments generally indicate that the interactions occur in two possible scenarios: (1) adsorption of polymer to the membrane surface, which is observed in all types of Pluronics, and (2) insertion of more hydrophobic polymers into the membrane. Although these observations appear consistent among experiments, a clear understanding of the mechanisms and driving forces that facilitate Pluronic−membrane interactions at atomic level remains elusive.

Computations provide an independent route to understanding detailed Pluronic−lipid membrane interactions. Interactions have been investigated by several studies using molecular dynamics (MD) and Monte Carlo simulations at different length and time scales.[13,20−24] Recently, for example, Rabbel et al.[20] conducted coarse-grained MC simulations and showed that full insertion with hydrophilic ends of the polymer on opposing sides of the membrane can lead to increased

Received: June 27, 2016
Revised: September 2, 2016
Published: September 13, 2016

DOI: 10.1021/acs.langmuir.6b02360
Langmuir 2016, 32, 10026−10033

permeability and pore formation, whereas partial insertion with hydrophilic ends on the same side of membrane has little or no effect on permeability. Hezaveh and coauthors[13] observed membrane thinning with Pluronics percolation by coarse-grained MD. However, few atomistic MD studies on Pluronics and Pluronic−membrane interactions have been performed. To the best of our knowledge, the only all-atom force field for MD simulations for the smallest oligomers of both PEO and PPO was proposed by Smith et al.[25−27] The only atomistic MD study of Pluronic membrane interaction was done by Nawaz et al.[24] where authors reported membrane bending in a DMPC lipid bilayer upon insertion of the copolymer. However, the interaction of Pluronics with dioleylphosphatidylcholine (DOPC) bilayers has not been investigated computationally. With one double bond in its center and 18 carbons in each tail, DOPC is one of the most typical unsaturated lipid component of cell membranes.[28]

Here we investigate the integration of Pluronics within a DOPC lipid bilayer by all-atom molecular dynamics simulations. Specifically, we have chosen L61 and L64 type Pluronics for our simulations. Both types have 30 hydrophobic PO repeating units. However, L61 has only two hydrophilic EO units at each end whereas L64 has 13. That is, the HLB (hydrophilic−lipophilic balance) for L61 and L64 is 1.8 and 14.5, respectively. The general OPLS all atom force field is modified and compared to the OPLS all atom force field specifically developed for Pluronics by Smith et al.[25−27] In particular, we examine the effect of the presence of copolymers on the structural and dynamic properties of DOPC.

COMPUTATIONAL METHODS

All MD simulations were performed using the GROMACS software package (version 5.0.4)[29] in the NPT ensemble with a time step of 2 ps. Coulombic interactions were calculated by the particle-mesh Ewald (PME) method[30,31] using a 1.1 nm cutoff for real space, a 0.12 nm grid spacing, and fourth-order interpolation. The van der Waals cutoff was set to 1.1 nm. The neighbor list was updated every 10 steps using a grid and 1.1 nm cutoff distance. All bonds were constrained using LINCS.[32,33] Temperature and pressure were controlled by the velocity rescale thermostat[34] and the Berendsen barostat[35] with a coupling time of 0.1 and 1.0 ps, respectively. Semi-isotropic pressure coupling was used with a reference pressure of 1 bar and a compressibility of 4.5×10^{-5} bar^{-1}, except for systems excluding the lipid bilayer where isotropic pressure coupling was applied. All simulations were energy minimized before the production runs using the steepest descent method.

Simulation of DOPC Lipid Bilayer. The Berger lipid model was implemented for use with the OPLS all atom (AA) force field[36] and TIP4P water.[37] Single lipid structures were initially obtained from the Automated Topology Builder and Repository Version 2.2.[38−40] 300 lipids were equally distributed over a grid in the upper and lower leaflets to form a symmetric bilayer; 14 226 water molecules were then randomly placed in this computational volume. The system was energy minimized before and after the addition of water. Production simulations were run for 70 ns. Properties were calculated by block averaging the last 50 ns, and local stress distributions were obtained using GROMACS-LS.[41−43]

Simulation of Pluronics. The OPLS-AA force field with partial charges obtained from density functional theory (DFT) calculations and the OPLS-AA type force field specifically developed for Pluronics by Smith et al.[25−27] were tested. The TIP4P water model was used with both force fields. Smith's force-field parameters were implemented into GROMACS through the use of tabulated potentials. DFT calculations were performed via Gaussian 03[44] using the B3LYP functional and a basis set of 6-311+G (3df,3pd). The charges were calculated by CHelpG.[45] Two short oligomers, each containing 3 PEO and 3 PPO monomers, were modeled. The oligomers were capped with methoxy groups and solvated in water. Very slight modifications to charges were made to neutralize the PEO and PPO monomers (cf. Table 1).

Table 1. Partial Charge Values for PEO and PPO Constituents Obtained from DFT Calculations

		charge value
PEO	C	0.372
	O	−0.660
	H	−0.021
PPO	C(CH)	0.640
	C(CH2)	0.100
	C(CH3)	−0.410
	O	−0.670
	H(CH)	−0.026
	H(CH2)	0.033
	H(CH3)	0.100
methoxy group	$O_{methoxy}$	−0.575
	$C_{methoxy}$	0.200
	$H_{methoxy}$	0.015

L61 and L64 were chosen for the molecular dynamics simulations. To compute the radius of gyration (R_g), a single chain of Pluronic was simulated for 70 ns in a simulation box containing ∼32 878 water molecules. The temperature was set to 300 K for L61 and to 280, 300, and 308 K for L64. To compute the density of the Pluronics melt, 300 initially randomly distributed chains were simulated at 300 K for 70 ns. All properties were calculated using the last 50 ns of the trajectories.

Simulation of Pluronics with DOPC Bilayer. Equilibrated single chains or five chains of Pluronics were solvated in an equilibrated DOPC bilayer/water system. For single chains of Pluronics three different starting configurations were tested: Pluronics placed (1) away from the lipid bilayer, (2) inside one of the lipid leaflets and close to the bilayer surface, and (3) in the middle of the bilayer. For five Pluronics chains, all Pluronics were randomly placed in the middle of the bilayer. The temperature was maintained at 300 or 310 K. All simulations ran for 500 ns. All properties were obtained by block averaging the trajectories.

Analysis. *Radius of Gyration.* One important parameter in polymer modeling is the radius of gyration (R_g), which can also be measured experimentally. It is a measure of a polymer chain dimension with the following mathematical definition:

$$R_g = \left(\frac{\sum_i \| r_i \|^2 m_i}{\sum_i m_i} \right)^{1/2}$$

where m_i is the mass and $\mathbf{r}_i$ is the position of atom i with respect to the center of mass of the molecule.

Diffusivity. Diffusivity is the measure of the diffusion rate. It is calculated from the mean-square displacements:

$$D(t) = \frac{1}{aNt} \left\langle \sum_{i=1}^{N} [r_i(t + t_0) - r_i(t_0)]^2 \right\rangle$$

where N is the number of molecules, t is the time, $\mathbf{r}_i$ is the center-of-mass position of molecule i, and $a = 2$ or 4 for one- or two-dimensional system, respectively.

Density Distribution. The mass density distribution of atoms is calculated for the DOPC phosphorus head groups and the Pluronics to identify the location of Pluronics with respect to the bilayer. Also, the thickness of the bilayer is calculated from the distance of the phosphorus peaks (D_{P-P}) in atom density distributions across the bilayer.

Radial Distribution Function. The radial distribution function is an important structural parameter that provides a general picture of how the density of atoms is distributed around a reference atom as a

DOI: 10.1021/acs.langmuir.6b02360
Langmuir 2016, 32, 10026−10033

function of distance. The intermolecular center-of-mass radial distribution functions are calculated for Pluronics:

$$g(r) = \frac{V}{4\pi r^2} \sum_i \sum_{j<i} P(r)$$

where V is the volume and $P(r)$ is the probability of finding molecule j at a distance r from molecule i.

RESULTS AND DISCUSSION

Structural Properties of the DOPC Lipid Bilayer Model. The structural properties of the Berger lipid model are first validated against experiments. For this purpose, 300 lipids are initially equally distributed over a grid in the upper and lower leaflets and then the system is relaxed in the presence of water molecules. This configuration avoids any asymmetric stress from forming across the bilayer which could change membrane permeability. Resulting 3D local pressure distributions are given in Figure 1.

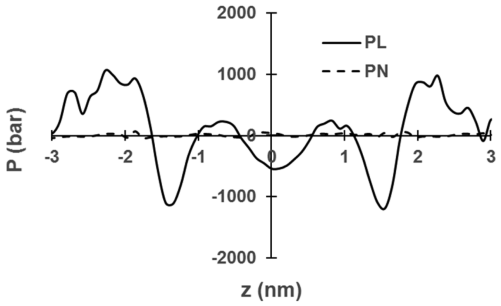

Figure 1. Stress profile for the DOPC bilayer system simulated at 300 K. Averages obtained from the last 50 ns of the trajectory. P_L and P_N are the lateral and normal components of the bilayer, respectively, as follows: $P_N = -\sigma_{zz}$ and $P_L = -(\sigma_{xx} + \sigma_{yy})/2$.

Structural Properties of Pluronics. Computed model lipid properties at 300 K are given in Table 2. The bilayer

Table 2. Properties of Model DOPC Lipid Bilayer Compared to the Experimental Findings

	membrane thickness (nm)	area per lipid headgroup (nm^2)	lateral diffusion coeff ($\mu m^2/s$)
Berger lipid	3.57 ± 0.25	7.02 ± 0.06	10.1 at 300 K
experimental	3.53–3.89[46–50]	6.69–7.30[46–51]	9.32 at 298 K[52]
			11.5 at 303 K[52]
			13.7 at 308 K[52]
			16.0 at 313 K[52]

thickness and area per lipid headgroup are calculated as 3.57 and 0.702 nm^2, respectively, in good agreement with experimental data obtained from combined neutron and X-ray scattering.[46–51] The lateral diffusion coefficient at 300 K (and 54 wt % of water) is computed as 10.1 $\mu m^2/s$, in good agreement with 10.2 $\mu m^2/s$ calculated by linear fitting of the experimental data (at 55 wt % of water) reported by Filippov et al.[52]

To test whether the original OPLS-AA force field with modified charges can be used to model the copolymers, we simulated dilute solutions of L64 at 280, 300, and 308 K and compared the R_g with the corresponding values obtained from the OPLS-AA force field developed by Smith et al.[25–27] as well as from experiments (cf. Table 3). In general, the R_g obtained

Table 3. Structural Properties of L61 and L64 Obtained from OPLS-AA Force Field Compared to Reported Experimental Results

	Pluronic type	temp (K)	R_g (nm)	density of melt (kg/m^3)
OPLS-AA with charges obtained from DFT calculations	L61	300	1.35 ± 0.22	
	L64	280	1.75 ± 0.40	
		300	1.78 ± 0.26	1013 ± 4
		308	1.91 ± 0.28	
Smith et al.[25–27]	L61	300	1.14 ± 0.23	
	L64	280	1.32 ± 0.21	
		300	1.39 ± 0.22	
		308	1.67 ± 0.33	
experimental	L61	300		1010[55]
	L64	280[53]	1.80	
		308[54]	1.85	

from the original OPLS-AA force field matches better with the experimental findings than the R_g using Smith's force field.[25–27] The values of R_g = 1.75 nm at 280 K and R_g = 1.91 nm at 308 K calculated from the original OPLS-AA force field simulations are in good agreement with dynamic light scattering[53] and small-angle neutron diffraction[54] experimental results of 1.80 nm (at 280 K) and 1.85 nm (at 308 K), respectively. In addition, for simulations using both force fields, the R_g for L61 is lower than for L64 due to the shorter PEO block size and lower molecular weight. Increasing the temperature increases R_g and the polymer chains become more extended. To the best of our knowledge, no experimental R_g has been reported for L61. Therefore, we additionally computed the melt density for L61 using the original OPLS-AA force field. The density of 1.013 ± 0.004 kg/L is obtained, in good agreement with the reported density of 1.01 kg/L.[55]

Pluronics–Membrane Interactions. It has been reported that L61 and L64 increase biomembrane permeation by inducing disturbance and pore formation.[56,57] Based on these experimental observations, together with the reported experimental high binding constants,[24] it is assumed that L61 and L64 can insert into the bilayer. Consequently, in a real system L61 and L64 are expected to bind to the membrane first and then gradually insert into the bilayer. However, it may not be possible to access the relevant experimental times with atomistic MD. Hence, due to the time restrictions of the simulations inherent to MD and supported by the assumption given above, in this study three different configurations were tested at 310 K. Single polymer chains are initially located (1) ~3.5 nm above the preformed bilayer (Figure 2A), (2) inside the upper or lower leaflet and close to bilayer surface (Figure 2D), and (3) at the center of the bilayer (Figure 2G). Density distributions of the copolymer with respect to the bilayer are calculated for each case and given in Figure 3. Full insertion of copolymers into the bilayer from the water is not observed within 500 ns simulation time. Yet both copolymers come in contact with the bilayer surface (Figure 3A). While the interaction is between the hydrophobic part of the polymer and the hydrophilic head groups of the bilayer for L61 (Figure 2B), L64 interacts with the hydrophilic ends (Figure 2C). After visual inspection of the trajectory, some membrane bending is also detected when L64 contacts the membrane surface. Because of the small size of atomistic simulations and the

DOI: 10.1021/acs.langmuir.6b02360
Langmuir 2016, 32, 10026–10033

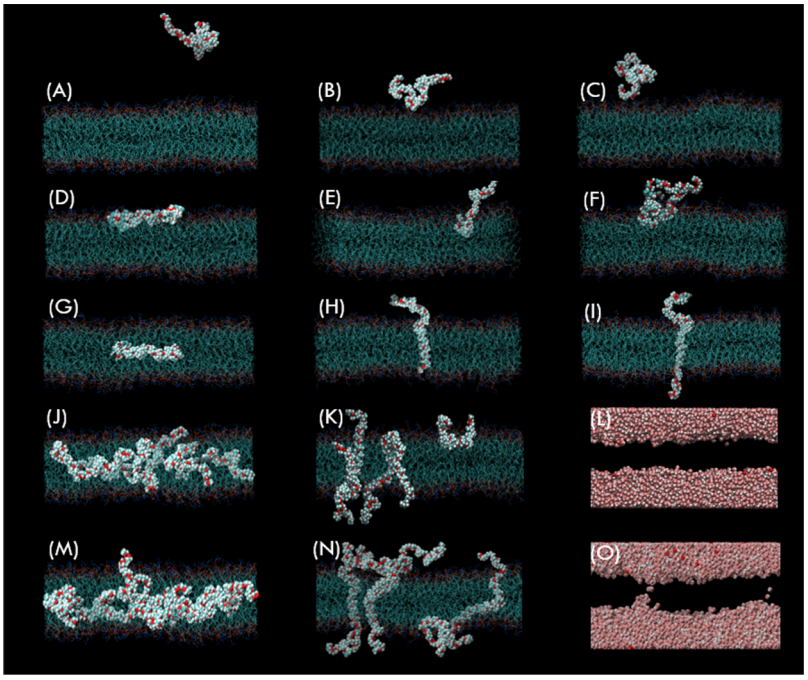

Figure 2. Initial and final configurations of Pluronics with respect to the bilayer. Single L61 or L64 chains are initially placed (A) away from the DOPC bilayer, (D) inside one of the leaflets close to the water/lipid interface, and (G) at the center of the bilayer. After 500 ns simulation time, the final configuration of L61 inside bilayer is given by (B), (E), (H) and for L64 by (C), (F), (I), when the polymer is initially placed as in (A), (D), (G), respectively. The polymers partially insert to the bilayer with PEO blocks being on the side, when the polymer is initially placed close to water/bilayer interface. On the other hand, the polymers span across the bilayer when they are initially centered within the bilayer. Concentration effect is investigated by randomly placing five Pluronic chains of (J) L61 and (M) L64 inside the bilayer. After 500 ns simulation time, the number of polymers that span across the bilayer is more with (K) L61 than (N) L64. However, unlike with (L) L61, the onset of pore formation is observed with (O) L64. For clarity, water is not shown in (A)−(N), but only water is shown in (L) and (O).

limitations imposed by periodic boundary conditions, this cannot be studied in detail here. Second, when the polymer is initially placed inside one of the leaflets, a U-shaped conformation is observed (or hook-shaped for L61) with PEO blocks being on the same side of the bilayer and PPO block being inside the membrane (Figure 2E,F). The insertion of L64 inside the bilayer is found to be shallower compared to that of L61 due to the longer PEO block size and hence stronger hydrophilic interactions (Figure 3 B). Third, when the polymer is initially centered inside the bilayer, both L61 and L64 span the membrane with PEO blocks being on opposite sides of the bilayer (Figure 2H,I). While L64 is mostly centered and crosses the bilayer at each hydrophilic side (≠-shape), L61 crosses the bilayer only from one side (T-shape) due to the smaller polymer size and weaker hydrophilic interactions (Figure 3C). The density distribution profiles of water across the lipid bilayer (Figure 3F) reveal that transmembrane configuration facilitates water transport across the bilayer, while no passage of water molecules is observed with U-shaped configuration. In addition, the penetration of water molecules inside DOPC is found to be more evident with L64 than L61. This is attributed to the lower binding preference of L64 to DOPC as given the radial distribution profiles of DOPC around each polymer in Figure 3G. It appears that the polymer lipid complex is more densely packed in the transmembrane case than in the U-shaped case which probably stems from the larger local disturbance imparted by the sharp kink in the polymer.

The polymer size and dynamics in the presence of a bilayer, as well as structural and dynamic properties of the bilayer in the presence of Pluronics, are monitored by calculating the R_g and end-to-end distance of the polymer, bilayer thickness, area per lipid head group, and lateral diffusion coefficient of the bilayer as well as the polymer. The results are listed in Table 4. Compared to the simulation results of a solely hydrated bilayer, greater thickness and lower lateral diffusion coefficient values are obtained for DOPC with the first Pluronics configuration indicating that the bilayer morphology changes in the presence of the copolymers. Lee and Firestone[58] observed dehydration upon introduction of Pluronics into the bilayer system; it is also known that membrane dehydration increases bilayer thickness and reduces the lateral diffusion coefficients.[59,60] On the other hand, when the polymer is initially placed inside the bilayer, the thickness of the membrane decreases. Reduced thickness values indicate a thinning effect of the polymer on the bilayer which is also reported by Lee and Firestone.[58] The difference is more evident when the copolymers diagonally cross the bilayer due to the compression induced by the two opposing PEO blocks. In addition, the lateral diffusion coefficient of the bilayer is slightly higher in the presence of the copolymer in agreement with experiments,[10] indicating membrane fluidity increases in the presence of the copolymers.

Similar to the condition observed for bilayers, both single chains of L61 and L64 become more compact, and the radius of gyration decreases in the presence of a bilayer compared to the no bilayer case when the polymer is still outside the DOPC. We attribute this behavior to the lower hydration levels of the polymer compared to the Pluronic/water binary system simulations. Once inside the bilayer, however, the copolymers adopt a more extended shape. The R_g values are 1.53 ± 0.17 nm for L61 and 2.00 ± 0.27 nm for L64 when the copolymer adopts a U-shaped (or hook-shaped) configuration. R_g increase to 1.82 ± 0.15 and 2.42 ± 0.22 nm for L61 and L64,

DOI: 10.1021/acs.langmuir.6b02360
Langmuir 2016, 32, 10026−10033

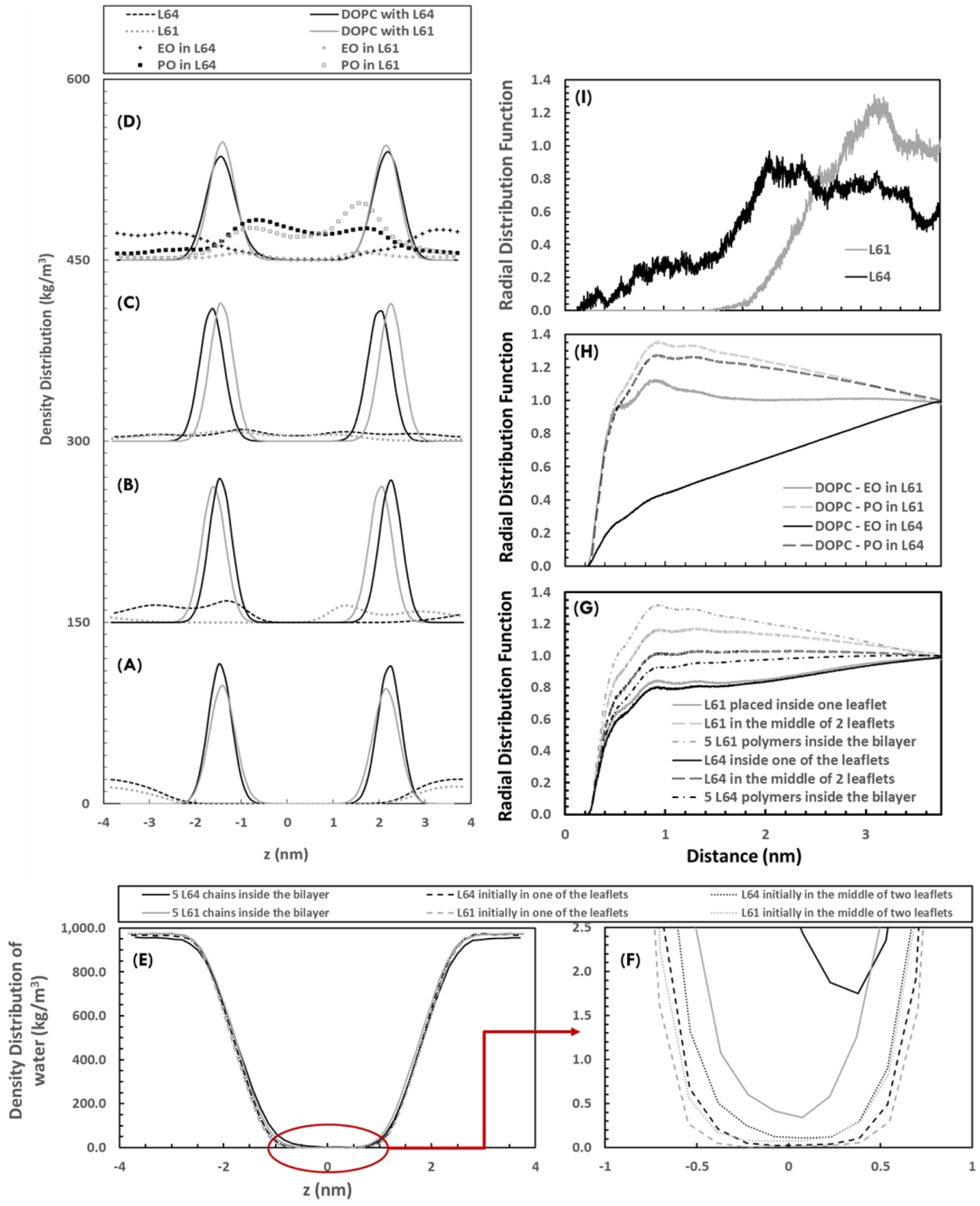

Figure 3. Density distribution of Pluronics with respect to the DOPC P−P head group when Pluronics initially placed (A) away from the bilayer, (B) at the water/bilayer interface, and (C) at the center of the bilayer. Partial integration of the copolymer to the bilayer is observed when Pluronic is initially located at the interface, whereas full insertion is detected when the copolymer is initially centered inside the bilayer. At high polymer concentrations, distribution of PEO and PPO blocks with respect to bilayer head groups is given in (D). The highest PEO distribution remains inside the hydrophilic region of the bilayer for L61 while it is within the water region for L64. Density distribution of water inside the bilayer for both Pluronics with all configurations is given in (E). Scales are enlarged in (F) for better visualization. Presence of L64 and transmembrane configuration facilitates water permeation inside DOPC. Radial distribution functions of DOPC are illustrated around each polymer (G) and for systems with multiple Pluronics around EO and PO groups of the polymers (H). The center-of-mass radial distribution function for L61 and L64 in a plane perpendicular to the bilayer normal is given in (I). Clustering of L64 is observed with the DOPC.

DOI: 10.1021/acs.langmuir.6b02360
Langmuir 2016, 32, 10026−10033

Table 4. Structural and Dynamic Properties of DOPC Lipid Bilayer in the Presence of Pluronics L61 and L64

	L61				L64			
	config1[a]	config2[b]	config3[c]	config4[d]	config1[a]	config2[b]	config3[c]	config4[d]
membrane thickness (nm)	3.76 ± 0.27	3.76 ± 0.24	3.73 ± 0.23	3.55 ± 0.29	3.76 ± 0.26	3.69 ± 0.23	3.68 ± 0.23	3.63 ± 0.30
area per lipid headgroup (nm^2)	7.08 ± 0.06	7.12 ± 0.06	7.15 ± 0.06	7.52 ± 0.07	7.08 ± 0.06	7.14 ± 0.06	7.18 ± 0.07	7.48 ± 0.08
lateral diffusion coeff of DOPC ($\mu m^2/s$)	9.9 ± 2.9	11.4 ± 0.2	18.6 ± 10.5	17.1 ± 0.6	7.4 ± 3.2	8.5 ± 2.4	10.6 ± 0.1	11.7 ± 5.7
radius of gyration of polymer(s) (nm)	1.33 ± 0.23	1.53 ± 0.17	1.82 ± 0.15	1.62 ± 0.09	1.78 ± 0.33	2.00 ± 0.27	2.42 ± 0.22	2.21 ± 0.08
end-to-end distance of polymer(s) (nm)	3.31 ± 1.32	3.98 ± 1.08	5.43 ± 0.78	3.72 ± 0.82[e] 5.48 ± 0.80[f] 4.54 ± 1.14[g]	4.25 ± 1.58	4.44 ± 1.55	7.35 ± 1.02	2.79 ± 1.06[e] 7.54 ± 1.18[f] 5.70 ± 2.35[g]
lateral diffusivity of polymer ($\mu m^2/s$)				19.8 ± 3.0				5.2 ± 0.6
diffusivity of polymer in z direction ($\mu m^2/s$)				2.1 ± 0.5				1.2 ± 1.4

[a]Pluronic is initially placed ~3.5 nm above the preformed bilayer. [b]Pluronic is initially placed at the bilayer/water interface. [c]Pluronic is initially placed at the center of the bilayer. [d]Five Pluronic chains randomly placed inside the membrane. [e]The smallest value obtained for a single polymer with U-shaped configuration. [f]The largest value obtained for a single polymer with transmembrane configuration. [g]The average of five polymers.

respectively. Hence, the extension becomes more significant when the polymers span the membrane. Similarly, the end-to-end distance values for L61 and L64 are obtained as 3.98 ± 1.08 and 4.44 ± 1.55 nm, respectively, with U-shaped (or hook-shaped for L61) configuration, and as 5.43 ± 0.78 and 7.35 ± 1.02 nm, respectively, with a transmembrane configuration. This indicates that both polymers assume an extended form in the transmembrane configuration. The difference is not significant for L61, though, due to smaller size of the polymer which causes the polymer to attain partial configurations (i.e., hook- and T-shaped) with the two initial starting configurations.

In general, no significant difference is observed in the area per lipid or in the diffusivity of the polymer in lateral and z directions (i.e., parallel to the bilayer normal) with single polymer chains which could be due to the small Pluronics/lipid ratio. Therefore, to understand the collective effect of Pluronics on the bilayer, five polymer chains of L61 or L64 were randomly distributed inside the bilayer (Figure 2J,M). Density distribution of PEO and PPO blocks with respect to bilayer P–P groups are given in Figure 3D. With both types of Pluronics, U-shaped and transmembrane configurations are observed together after 500 ns, with the transmembrane configuration more dominant. That is, 3 and 4 (out of 5) chains have attained the transmembrane configuration with L64 and L61, respectively. In addition, the water density distribution profiles inside the bilayer indicate that more than 5× water density is attained with L64 compared to L61 (Figure 3E,F). Analysis of the trajectories clearly reveals the onset of pore formation with L64 (Figure 2O), but not with L61 (Figure 2L) during the simulations. Figure 3G shows that the binding preference of L61 to DOPC is much higher than L64. Unlike with L64, with L61 both EO and PO groups play a major role in this binding (Figure 3H). Consequently, no pore formation with L61 could be due the strong EO interactions of L61 with the hydrophilic heads of the bilayer. After analyzing the whole trajectories, we observe that Pluronics induce bending and local thinning in the DOPC bilayer in accordance with the findings reported for DMPC.[24] The bilayer membrane thickness decreases from 3.76 nm, when the polymer is outside the bilayer, to 3.55 and 3.63 nm respectively in the presence of L61 and L64. While the bilayer thickness decreases, the area per lipid headgroup increases as expected (Table 4). Moreover, the lateral diffusivity of the bilayer increases in the presence of Pluronics similar to the single chain simulations. However, within error, no significant differences are observed in the areas and lateral diffusivities of the bilayer including L61 or L64 or in the diffusivities of L61 and L64 parallel to the membrane normal. The average R_g and end-to-end distances of the polymers attain a value between the R_g and end-to-end distance values of the single polymer simulations with initial configurations 2 and 3 (Table 4). This is attributed to the existence of both U-shaped and transmembrane configurations as well as the decrease in bilayer thickness. In a thinner membrane, the extension of the PPO block, and hence the polymer R_g in the bilayer, are expected to be less than in transmembrane configurations in single polymer simulations. Finally, the lateral diffusivity of L61 in DOPC is much higher than that of L64. Whereas the lateral diffusivity of L61 is close to membrane lateral diffusivity indicating both move together, the lateral diffusivity of L64 is much smaller than that of the membrane. The center-of-mass plots around the plane diagonal to the membrane normal reveal that L64 forms clusters in the bilayer whereas L61 does not (Figure 3I).

SUMMARY AND CONCLUSIONS

We investigated the interaction mechanism of Pluronics of different HLB with a DOPC lipid bilayer though atomistic MD. We used L61- and L64-type Pluronics and modified the charges of PEO and PPO blocks though DFT calculations for use with the OPLS-AA force field. Single polymer chains were initially placed (1) far from the bilayer, (2) at the bilayer/water interface, and (3) at the center of the bilayer, and their conformations with respect to the bilayer were monitored. No insertion of the polymers into the bilayer is detected for the first initial configuration. However, L61 and L64 adsorb to the surface of the bilayer through PPO and PEO blocks, respectively. With the second initial configuration both Pluronics partially insert into the bilayer, resulting in a U-shaped (hook-shaped for L61) conformation. Finally, from the third initial configuration polymers fully insert into the bilayer achieving a transmembrane shape. In general, in the presence of Pluronics, the membrane thickness decreases and its fluidity increases in agreement with experimental observations.[10,58] Specifically, the transmembrane configuration induces more local thinning and membrane bending. Second, the collective

DOI: 10.1021/acs.langmuir.6b02360
Langmuir 2016, 32, 10026–10033

effect of the copolymers was investigated by randomly placing five polymer chains inside the bilayer. In these simulations, the decrease in membrane thickness and the increase in membrane fluidity become more pronounced. Unlike L61, L64 is found to cluster inside the bilayer. Finally, at higher polymer concentrations, L64 can form pores inside the bilayer as recently reported by Chen et al.[56] However, no pore formation is detected with L61 during the span of the simulations. Pore formation in the presence of L64 can greatly facilitate molecular transport across cellular membranes. The delivery of drugs encapsulated inside the liposomes can be controlled by introducing the copolymers into these systems without inducing complete disruption of the bilayer, as previously suggested.[11]

In conclusion, our results indicate that HLB in polymers defines the interaction mechanism of the polymer with the bilayer as well as the dynamics of the polymer within the bilayer. These findings therefore provide an understanding of underpinning molecular mechanisms and have potential to improve drug delivery systems.

AUTHOR INFORMATION

Corresponding Author

*E-mail rfaller@ucdavis.edu (R.F.).

Notes

The authors declare no competing financial interest.

ACKNOWLEDGMENTS

This work was supported by a Grant from the University of California Office of the President UCOP Lab Fee Program (Grant 12-LR-237353) and was partially performed under the auspices of the U.S. Department of Energy by Lawrence Livermore National Laboratory under Contract DE-AC52-07NA27344. Computations were performed at LLNL Aztec and Sierra massively parallel computers. Analysis were partially performed at TUBITAK ULAKBIM, High Performance and Grid Computing Center (TRUBA resources).

REFERENCES

(1) Cambón, A.; Rey-Rico, A.; Barbosa, S.; Soltero, J. F. A.; Yeates, S. G.; Brea, J.; Loza, M. I.; Alvarez-Lorenzo, C.; Concheiro, A.; Taboada, P.; Mosquera, V. Poly(styrene oxide)-poly(ethylene oxide) block copolymers: From "classical" chemotherapeutic nanocarriers to active cell-response inducers. *J. Controlled Release* **2013**, *167*, 68−75.

(2) Yasuda, S.; Townsend, D.; Michele, D. E.; Favre, E. G.; Day, S. M.; Metzger, J. M. Dystrophic heart failure blocked by membrane sealant poloxamer. *Nature* **2005**, *436*, 1025−1029.

(3) Kabanov, A. V.; Alakhov, V. Y. Pluronic® block copolymers in drug delivery: From micellar nanocontainers to biological response modifiers. *Crit. Rev. Ther. Drug Carrier Syst.* **2002**, *19*, 1.

(4) Huang, J.; Zhang, H.; Yu, Y.; Chen, Y.; Wang, D.; Zhang, G.; Zhou, G.; Liu, J.; Sun, Z.; Sun, D. Biodegradable self-assembled nanoparticles of poly (d, l-lactide-co-glycolide)/hyaluronic acid block copolymers for target delivery of docetaxel to breast cancer. *Biomaterials* **2014**, *35*, 550−566.

(5) Torcello-Gómez, A.; Wulff-Pérez, M.; Gálvez-Ruiz, M. J.; Martín-Rodríguez, A.; Cabrerizo-Vílchez, M.; Maldonado-Valderrama, J. Block copolymers at interfaces: Interactions with physiological media. *Adv. Colloid Interface Sci.* **2014**, *206*, 414−427.

(6) Hira, S. K.; Ramesh, K.; Gupta, U.; Mitra, K.; Misra, N.; Ray, B.; Manna, P. P. Methotrexate-Loaded Four-Arm Star Amphiphilic Block Copolymer Elicits CD8+ T Cell Response against a Highly Aggressive and Metastatic Experimental Lymphoma. *ACS Appl. Mater. Interfaces* **2015**, *7*, 20021−20033.

(7) Kabanov, A.; Zhu, J.; Alakhov, V. Pluronic Block Copolymers for Gene Delivery. In *Advances in Genetics*; Academic Press: 2005; Vol. *53*, pp 231−261.

(8) Sharma, A. K.; Zhang, L.; Li, S.; Kelly, D. L.; Alakhov, V. Y.; Batrakova, E. V.; Kabanov, A. V. Prevention of MDR development in leukemia cells by micelle-forming polymeric surfactant. *J. Controlled Release* **2008**, *131*, 220−227.

(9) Cheng, C.-Y.; Wang, J.-Y.; Kausik, R.; Lee, K. Y. C.; Han, S. Nature of interactions between PEO-PPO-PEO triblock copolymers and lipid membranes:(II) role of hydration dynamics revealed by dynamic nuclear polarization. *Biomacromolecules* **2012**, *13*, 2624−2633.

(10) Krylova, O. O.; Melik-Nubarov, N. S.; Badun, G. A.; Ksenofontov, A. L.; Menger, F. M.; Yaroslavov, A. A. Pluronic L61 accelerates flip−flop and transbilayer doxorubicin permeation. *Chem. - Eur. J.* **2003**, *9*, 3930−3936.

(11) Rahman, M.; Yu, E.; Forman, E.; Roberson-Mailloux, C.; Tung, J.; Tringe, J.; Stroeve, P. Modified release from lipid bilayer coated mesoporous silica nanoparticles using PEO−PPO−PEO triblock copolymers. *Colloids Surf., B* **2014**, *122*, 818−822.

(12) Wang, J.-Y.; Chin, J.; Marks, J. D.; Lee, K. Y. C. Effects of PEO−PPO− PEO triblock copolymers on phospholipid membrane integrity under osmotic stress. *Langmuir* **2010**, *26*, 12953−12961.

(13) Hezaveh, S.; Samanta, S.; De Nicola, A.; Milano, G.; Roccatano, D. Understanding the interaction of block copolymers with DMPC lipid bilayer using coarse-grained molecular dynamics simulations. *J. Phys. Chem. B* **2012**, *116*, 14333−14345.

(14) Hädicke, A.; Blume, A. Interactions of Pluronic block copolymers with lipid monolayers studied by epi-fluorescence microscopy and by adsorption experiments. *J. Colloid Interface Sci.* **2013**, *407*, 327−338.

(15) Firestone, M. A.; Wolf, A. C.; Seifert, S. Small-angle X-ray scattering study of the interaction of poly (ethylene oxide)-b-poly (propylene oxide)-b-poly (ethylene oxide) triblock copolymers with lipid bilayers. *Biomacromolecules* **2003**, *4*, 1539−1549.

(16) Wang, J.; Segatori, L.; Biswal, S. L. Probing the association of triblock copolymers with supported lipid membranes using micro-cantilevers. *Soft Matter* **2014**, *10*, 6417−6424.

(17) Hädicke, A.; Blume, A. Interactions of Pluronic block copolymers with lipid vesicles depend on lipid phase and Pluronic aggregation state. *Colloid Polym. Sci.* **2015**, *293*, 267−276.

(18) Melik-Nubarov, N.; Pomaz, O.; Dorodnych, T. Y.; Badun, G.; Ksenofontov, A.; Schemchukova, O.; Arzhakov, S. Interaction of tumor and normal blood cells with ethylene oxide and propylene oxide block copolymers. *FEBS Lett.* **1999**, *446*, 194−198.

(19) Wu, G.; Majewski, J.; Ege, C.; Kjaer, K.; Weygand, M. J.; Lee, K. Y. C. Interaction between lipid monolayers and poloxamer 188: an X-ray reflectivity and diffraction study. *Biophys. J.* **2005**, *89*, 3159−3173.

(20) Rabbel, H.; Werner, M.; Sommer, J.-U. Interactions of Amphiphilic Triblock Copolymers with Lipid Membranes: Modes of Interaction and Effect on Permeability Examined by Generic Monte Carlo Simulations. *Macromolecules* **2015**, *48*, 4724−4732.

(21) Nawaz, S.; Carbone, P. Coarse-Graining Poly (ethylene oxide)−Poly (propylene oxide)−Poly (ethylene oxide) (PEO−PPO−PEO) Block Copolymers Using the MARTINI Force Field. *J. Phys. Chem. B* **2014**, *118*, 1648−1659.

(22) Frey, S. L.; Zhang, D.; Carignano, M. A.; Szleifer, I.; Lee, K. Y. C. Effects of block copolymer's architecture on its association with lipid membranes: experiments and simulations. *J. Chem. Phys.* **2007**, *127*, 114904.

(23) Hatakeyama, M.; Faller, R. In *Coarse Grained Simulation of Lipid Membrane and Triblock Copolymers*; COMPLEX SYSTEMS: 5th International Workshop on Complex Systems; AIP Publishing: 2008; pp 528−531.

(24) Nawaz, S.; Redhead, M.; Mantovani, G.; Alexander, C.; Bosquillon, C.; Carbone, P. Interactions of PEO−PPO−PEO block copolymers with lipid membranes: a computational and experimental study linking membrane lysis with polymer structure. *Soft Matter* **2012**, *8*, 6744−6754.

DOI: 10.1021/acs.langmuir.6b02360
Langmuir 2016, 32, 10026−10033

(25) Smith, G. D.; Borodin, O.; Bedrov, D. Quantum Chemistry Based Force Field for Simulations of Poly (propylene oxide) and Its Oligomers. *J. Phys. Chem. A* **1998**, *102*, 10318−10323.
(26) Bedrov, D.; Pekny, M.; Smith, G. D. Quantum-chemistry-based force field for 1, 2-dimethoxyethane and poly (ethylene oxide) in aqueous solution. *J. Phys. Chem. B* **1998**, *102*, 996−1001.
(27) Smith, G. D.; Borodin, O.; Bedrov, D. A revised quantum chemistry-based potential for poly (ethylene oxide) and its oligomers in aqueous solution. *J. Comput. Chem.* **2002**, *23*, 1480−1488.
(28) van Meer, G.; de Kroon, A. I. Lipid map of the mammalian cell. *J. Cell Sci.* **2011**, *124*, 5−8.
(29) Berendsen, H. J.; van der Spoel, D.; van Drunen, R. GROMACS: A message-passing parallel molecular dynamics implementation. *Comput. Phys. Commun.* **1995**, *91*, 43−56.
(30) Darden, T.; York, D.; Pedersen, L. Particle mesh Ewald: An N·log (N) method for Ewald sums in large systems. *J. Chem. Phys.* **1993**, *98*, 10089−10092.
(31) Essmann, U.; Perera, L.; Berkowitz, M. L.; Darden, T.; Lee, H.; Pedersen, L. G. A smooth particle mesh Ewald method. *J. Chem. Phys.* **1995**, *103*, 8577−8593.
(32) Hess, B.; Bekker, H.; Berendsen, H. J.; Fraaije, J. G. LINCS: a linear constraint solver for molecular simulations. *J. Comput. Chem.* **1997**, *18*, 1463−1472.
(33) Hess, B. P-LINCS: A parallel linear constraint solver for molecular simulation. *J. Chem. Theory Comput.* **2008**, *4*, 116−122.
(34) Bussi, G.; Donadio, D.; Parrinello, M. Canonical sampling through velocity rescaling. *J. Chem. Phys.* **2007**, *126*, 014101.
(35) Berendsen, H. J.; Postma, J. P. M.; van Gunsteren, W. F.; DiNola, A.; Haak, J. Molecular dynamics with coupling to an external bath. *J. Chem. Phys.* **1984**, *81*, 3684−3690.
(36) Tieleman, D. P.; MacCallum, J. L.; Ash, W. L.; Kandt, C.; Xu, Z.; Monticelli, L. Membrane protein simulations with a united-atom lipid and all-atom protein model: lipid−protein interactions, side chain transfer free energies and model proteins. *J. Phys.: Condens. Matter* **2006**, *18*, S1221.
(37) Jorgensen, W. L.; Chandrasekhar, J.; Madura, J. D.; Impey, R. W.; Klein, M. L. Comparison of simple potential functions for simulating liquid water. *J. Chem. Phys.* **1983**, *79*, 926−935.
(38) Malde, A. K.; Zuo, L.; Breeze, M.; Stroet, M.; Poger, D.; Nair, P. C.; Oostenbrink, C.; Mark, A. E. An automated force field topology builder (ATB) and repository: version 1.0. *J. Chem. Theory Comput.* **2011**, *7*, 4026−4037.
(39) Koziara, K. B.; Stroet, M.; Malde, A. K.; Mark, A. E. Testing and validation of the Automated Topology Builder (ATB) version 2.0: prediction of hydration free enthalpies. *J. Comput.-Aided Mol. Des.* **2014**, *28*, 221−233.
(40) Canzar, S.; El-Kebir, M.; Pool, R.; Elbassioni, K.; Malde, A. K.; Mark, A. E.; Geerke, D. P.; Stougie, L.; Klau, G. W. Charge group partitioning in biomolecular simulation. *J. Comput. Biol.* **2013**, *20*, 188−198.
(41) Vanegas, J. M.; Torres-Sánchez, A.; Arroyo, M. Importance of force decomposition for local stress calculations in biomembrane molecular simulations. *J. Chem. Theory Comput.* **2014**, *10*, 691−702.
(42) Torres-Sánchez, A.; Vanegas, J. M.; Arroyo, M. Examining the mechanical equilibrium of microscopic stresses in molecular simulations. *Phys. Rev. Lett.* **2015**, *114*, 258102.
(43) Ollila, O. S.; Risselada, H. J.; Louhivuori, M.; Lindahl, E.; Vattulainen, I.; Marrink, S. J. 3D pressure field in lipid membranes and membrane-protein complexes. *Phys. Rev. Lett.* **2009**, *102*, 078101.
(44) Frisch, M. J.; Trucks, G. W.; Schlegel, H. B.; Scuseria, G. E.; Robb, M. A.; Cheeseman, J. R.; Scalmani, G.; Barone, V.; Mennucci, B.; Petersson, G. A.; Nakatsuji, H.; Caricato, M.; Li, X.; Hratchian, H. P.; Izmaylov, A. F.; Bloino, J.; Zheng, G.; Sonnenberg, J. L.; Hada, M.; Ehara, M.; Toyota, K.; Fukuda, R.; Hasegawa, J.; Ishida, M.; Nakajima, T.; Honda, Y.; Kitao, O.; Nakai, H.; Vreven, T.; Montgomery, J. A., Jr.; Peralta, J. E.; Ogliaro, F.; Bearpark, M. J.; Heyd, J.; Brothers, E. N.; Kudin, K. N.; Staroverov, V. N.; Kobayashi, R.; Normand, J.; Raghavachari, K.; Rendell, A. P.; Burant, J. C.; Iyengar, S. S.; Tomasi, J.; Cossi, M.; Rega, N.; Millam, N. J.; Klene, M.; Knox, J. E.; Cross, J. B.; Bakken, V.; Adamo, C.; Jaramillo, J.; Gomperts, R.; Stratmann, R. E.; Yazyev, O.; Austin, A. J.; Cammi, R.; Pomelli, C.; Ochterski, J. W.; Martin, R. L.; Morokuma, K.; Zakrzewski, V. G.; Voth, G. A.; Salvador, P.; Dannenberg, J. J.; Dapprich, S.; Daniels, A. D.; Farkas, Ö.; Foresman, J. B.; Ortiz, J. V.; Cioslowski, J.; Fox, D. J. *Gaussian 03*; Gaussian, Inc.: Wallingford, CT, 2004.
(45) Breneman, C. M.; Wiberg, K. B. Determining atom-centered monopoles from molecular electrostatic potentials. The need for high sampling density in formamide conformational analysis. *J. Comput. Chem.* **1990**, *11*, 361−373.
(46) Kučerka, N.; Nagle, J. F.; Sachs, J. N.; Feller, S. E.; Pencer, J.; Jackson, A.; Katsaras, J. Lipid Bilayer Structure Determined by the Simultaneous Analysis of Neutron and X-Ray Scattering Data. *Biophys. J.* **2008**, *95*, 2356−2367.
(47) Pangali, C.; Rao, M.; Berne, B. J. On a Novel Monte Carlo Scheme for Simulating Water and Aqueous Solutions. *Chem. Phys. Lett.* **1978**, *55*, 413−417.
(48) Liu, Y.; Nagle, J. F. Diffuse scattering provides material parameters and electron density profiles of biomembranes. *Phys. Rev. E* **2004**, *69*, 040901.
(49) Tristram-Nagle, S.; Petrache, H. I.; Nagle, J. F. Structure and Interactions of Fully Hydrated Dioleoylphosphatidylcholine Bilayers. *Biophys. J.* **1998**, *75*, 917−925.
(50) Kučerka, N.; Gallová, J.; Uhríková, D.; Balgavý, P.; Bulacu, M.; Marrink, S.-J.; Katsaras, J. Areas of Monounsaturated Diacylphosphatidylcholines. *Biophys. J.* **2009**, *97*, 1926−1932.
(51) Nagle, J. F.; Tristram-Nagle, S. Structure of lipid bilayers. *Biochim. Biophys. Acta, Rev. Biomembr.* **2000**, *1469*, 159−195.
(52) Filippov, A.; Orädd, G.; Lindblom, G. Influence of Cholesterol and Water Content on Phospholipid Lateral Diffusion in Bilayers. *Langmuir* **2003**, *19*, 6397−6400.
(53) Chu, B. Structure and Dynamics of Block Copolymer Colloids. *Langmuir* **1995**, *11*, 414−421.
(54) Causse, J.; Oberdisse, J.; Jestin, J.; Lagerge, S. Small-Angle Neutron Scattering Study of Solubilization of Tributyl Phosphate in Aqueous Solutions of L64 Pluronic Triblock Copolymers. *Langmuir* **2010**, *26*, 15745−15753.
(55) van Gunsteren, W. F. Constrained dynamics of flexible molecules. *Mol. Phys.* **1980**, *40* (4), 1015−1019.
(56) Chen, J.; Luo, J.; Zhao, Y.; Pu, L.; Lu, X.; Gao, R.; Wang, G.; Gu, Z. Increase in transgene expression by Pluronic L64-mediated endosomal/lysosomal escape through its membrane-disturbing action. *ACS Appl. Mater. Interfaces* **2015**, *7*, 7282−7293.
(57) Krylova, O. O.; Pohl, P. Ionophoric Activity of Pluronic Block Copolymers. *Biochemistry* **2004**, *43*, 3696−3703.
(58) Lee, B.; Firestone, M. A. Electron density mapping of triblock copolymers associated with model biomembranes: Insights into conformational states and effect on bilayer structure. *Biomacromolecules* **2008**, *9*, 1541−1550.
(59) Lehtonen, J. Y.; Kinnunen, P. K. Changes in the lipid dynamics of liposomal membranes induced by poly(ethylene glycol): free volume alterations revealed by inter- and intramolecular excimer-forming phospholipid analogs. *Biophys. J.* **1994**, *66*, 1981−1990.
(60) Aeffner, S. *Stalk Structures in Lipid Bilayer Fusion Studied by X-ray Diffraction*; Universitätsverlag Göttingen: 2012; Vol. *6*.

DOI: 10.1021/acs.langmuir.6b02360
Langmuir 2016, 32, 10026−10033